Paleoaltimetry of Mio-Pliocene Camp Davis Formation, Gros Ventre Range, Wyoming: Stable Isotope Analysis of Lacustrine Carbonates

Skye Alexa Caplan

A Thesis submitted in partial fulfillment of
Requirements for
B.S. Honors in Earth and Environment Sciences
20 April 2020

Abstract

The importance of reconstructing paleoaltimetry in geological studies lies in how a location's topography affects its surroundings. Elevation impacts drainage patterns, atmospheric processes, and can influence the biodiversity of an area. In order to reconstruct paleoelevation, isotope analysis can be employed on carbonate proxy materials to estimate the isotopic composition of meteoric water whose composition changes with increasing elevation. Building off of the earlier study of Drummond et al. (1993), this study uses conventional isotope analysis of lacustrine carbonate to determine the paleoelevation of the Camp Davis Formation in the Gros Ventre Mountains, Wyoming. This formation represents a Miocene-age terrestrial depositional system comprising: a basal lithic conglomerate formed as alluvial fans; a middle limestone unit formed in a lacustrine setting; and an upper unit of terrestrial volcanic ash deposits.

Four hand samples were collected from the carbonate member and analyzed for their $\delta^{18}O$ and $\delta^{13}C$ content. Analysis of micritic matrix, lithoclasts, and cements define two distinct compositional populations based on $\delta^{18}O$: one at -18 and -15‰. The oxygen isotope values of these carbonates allows for estimation of the isotopic composition of meteoric water assuming a range of precipitational temperatures. Furthermore, given the general relation between $\delta^{18}O$ meteoric water and elevation, it is then possible to estimate the paleoelevation. Results from this study of the Camp Davis Fm. indicate a paleoelevation very close to present-day conditions, implying a long term balance between erosion and continued tectonic uplift. Importantly, this study contrasts significantly with interpretation of Drummond et al. (1993) that suggested elevations as much as 2 kilometers higher during the Miocene.

Introduction

In order to understand the geologic history of an area it is necessary to understand how the surface has evolved over time. Change in elevation, in particular, is one aspect of that is critical to understanding the processes and timing of tectonic deformation. In this light, when examining ancient settings, how is it possible to reconstruct paleoelevation? What records of elevation are preserved in the geologic record and how are they manifested? When considering changes in elevation, the dominant physical factors that vary as a function of altitude are atmospheric pressure and temperature. While geologic archives of ambient atmospheric pressure are elusive, numerous retrievable records are available to reconstruct paleotemperature in terrestrial settings.

Classically, changes in floral and faunal assemblages have been employed to provide large scale variation in surface temperature (Wing and Harrington, 2001). These biotic proxies of temperature are based on the concept that the ecological range of numerous taxonomic groups have not changed significantly over geologic time and can serve as an broad indicator of environmental conditions. This has more recently been revived as ecologic niche modelling research that quantitatively evaluates taxonomic assemblage member abundance to such parameters as temperature, water availability, etc. However, the resolution of temperature change is quite limited, on the order of 10's of degrees, which is unsuitable for ascertaining elevation to any reasonable level of acuity.

Geochemical proxies, however, offer an additional measure of altitude. For example, a strong relationship exists between the isotopic composition of hydrogen and oxygen in meteoric precipitation and altitude. It has been shown that with increasing altitude (and decreasing temperature), rainwater becomes progressively more depleted in δD and $\delta^{18}O$ (Drummond et al., 1993; Rowley and Garzione, 2007; Lechler et al., 2013). These techniques exploit a key relationship between altitude and meteoric precipitation. As altitude increases, heavy, ^{18}O-enriched molecules condense and precipitate out first, leaving lighter, ^{18}O-depleted meteoric water to rain down on higher elevations. As the cloud containing the water vapor is a limited reservoir, the change in composition can be modelled as a Rayleigh fractionation which leads to a progressive deletion with increasing elevation and rainout. This effect is enhanced by the increased fractionation as air temperature decreases as altitude increases. These changes in water composition must, however, be preserved in a proxy of the isotopic composition of meteoric water and paleotemperature. For example, where mountain glaciers remain, a record of these paleowaters can be recovered from ice cores that might extend back 10's of thousands of years (Jasechko et al., 2015). While measured changes in the isotopic composition this ice can allow reconstruction of variation in paleotemperature with temporal resolution at an annual scale, such records are limited to the last several hundred thousand years in the best of circumstances. Unfortunately, major changes in paleoelevation are unlikely to occur at such short timescales.

Traditionally, carbonate minerals have served as the primary material used in studies of this type. The oxygen isotope composition of carbonate is controlled by both the temperature of precipitation and the composition of the water from which it forms (Rowley and Garzione, 2007). In conventional stable isotope carbonate paleothermometery, the temperature relationship can be represented as the fractionation of $^{18}O/^{16}O$ between the precipitating mineral relative to the water from which it forms. This temperature relation is shown in Equation 1.

$$10^3 \ln(\alpha_{Cc-water}) = 2.78(10^6)(T^{-2}) - 2.89 \qquad \text{Eq. 1}$$

Utilizing this temperature relation and the calculated value of α, it then possible to relate the isotopic ratios of both phases (Equation 2) and when represented in delta (δ) notation, possible to estimate the composition of each phase when one is known or estimated (Equation 3)

$$\alpha_{Cc-water} = \frac{\left(\frac{^{18}O}{^{16}O}\right)_{Cc}}{\left(\frac{^{18}O}{^{16}O}\right)_{water}} \quad \text{Eq. 2}$$

$$\alpha_{Cc-water} = \frac{\delta^{18}O_{Cc}+1000}{\delta^{18}O_{water}+1000} \quad \text{Eq. 3}$$

From Equation 3, when measured carbonate values are known and a range of temperature can be constrained, it is then possible to estimate the isotopic composition of the water. Typically, the carbonate materials employed have included soil carbonate nodules or lacustrine carbonate which both form during the warmer summer months, and in turn limits the range of temperatures that need to be considered (Hren and Sheldon, 2012; Quade et al., 2007; Passey et al., 2014). Nevertheless, this assumption or constraint is not perfect, as the ideal solution of this relationship requires independent knowledge of water for determination of paleotemperature and thus paleoaltitude. A recently developed method offers promise for the direct estimation of precipitational temperature for carbonate minerals. This technique, the clumped isotope method, examines the abundance of doubly bonded rare isotopes, ^{13}C and ^{18}O, in the carbonate molecule as a function of temperature, independent of the composition of the water. Thus, clumped isotope analysis can provide an independent estimate of precipitational temperature which in turn allows direct calculation of water from measured $\delta^{18}O$ carbonate. This approach was intended for this study but because of the Covid-19 shutdown samples remain in the analytical que at this time.

As noted above, both methods require the isotope analysis of proxy materials representative of the area's precipitation, including lacustrine carbonates (Drummond et al., 1993), hydrous minerals (Gébelin et al., 2013), and biogenic carbonate (Kohn and Dettman, 2007). This study examines $\delta^{18}O$ of lacustrine carbonates of the Camp Davis Formation in northwestern Wyoming to estimate the formation's paleoelevation.

Geologic Setting:

The Camp Davis Formation outcrops in northwestern Wyoming bound by the Hoback Fault and Gros Ventre mountain range to the northeast (Fig.1). It is composed of multiple subunits defined by texture and composition. The lower Camp Davis Fm. is characterized by a calcareous conglomerate comprising lithoclasts derived from erosion and transport of the highlands of the Gros Ventre Mountains (Fig. 2). Locally, this conglomerate is overlain by a paleosol. Above the paleosol is a sequence of micritic limestones that are the focus of this study. These limestones consist of tan to brown colored micrites that coarsen upwards over the span of approximately 25 meters (Davis and Wilkinson 1983). The coarser layers are pisolitic grainstones that are cemented by a clear calcite spar. The formation is capped by a unit containing volcanic ash that has been correlated to the ash deposits in the nearby Teewinot Formation (Ritchie, 1981; Love, 1986). Based

on the Teewinot Formation's age of about 9.2 Ma, the Camp Davis Formation has been determined to be of late Miocene age (Evernden et al., 1964).

The carbonate sequence represents a lacustrine environment whose water was sourced by meteoric runoff from the adjacent Gros Ventre Mountains. The lowermost layer in the sequence is a homogenous calcareous mudstone that contains root molds and evidence of the aquatic algae *Chara*. These mudstones would have been deposited in a low energy marsh environment that existed near the lake's shore. The next layers consist of calcareous siltstone and sandstone which are homogenous and root mottled like the mudstones beneath them. The uppermost unit in the sequence is a calcareous sandstone that coarsens to a granule conglomerate and is overlain by lithologies containing abundant volcanic ash. The conglomerate contains carbonate clasts as well as *Chara* encrustations and volcanic fragments from nearby eruptions (Davis and Wilkinson 1983).

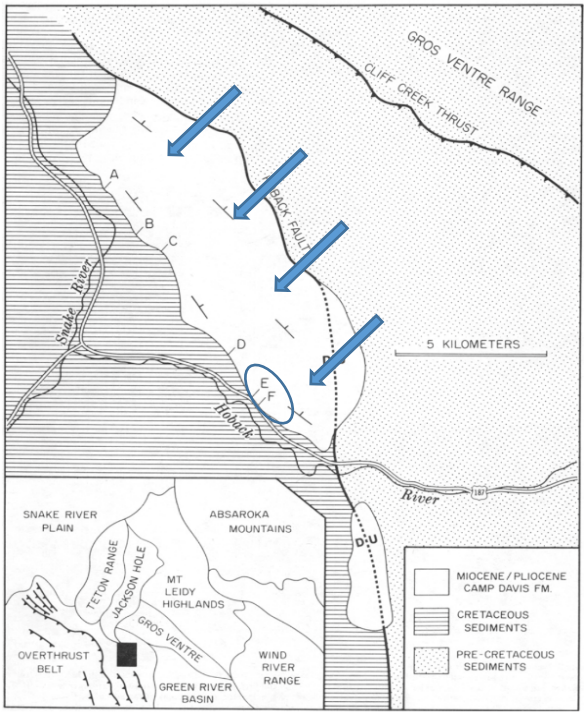

Figure 1: Location of Camp Davis Formation adjacent to the normal Hoback Fault that bounds the Southwestern edge of the Gros Ventre Mountains. Samples were taken from ridge adjacent to locations E and F (circled area). Active sediment transport from the uplifted block of Hoback Fault was to the Southwest and resulted in a thick sequence of basal conglomerates overlain by later lacustrine and ash beds. Figure is modified from Davis and Wilkinson, 1983.

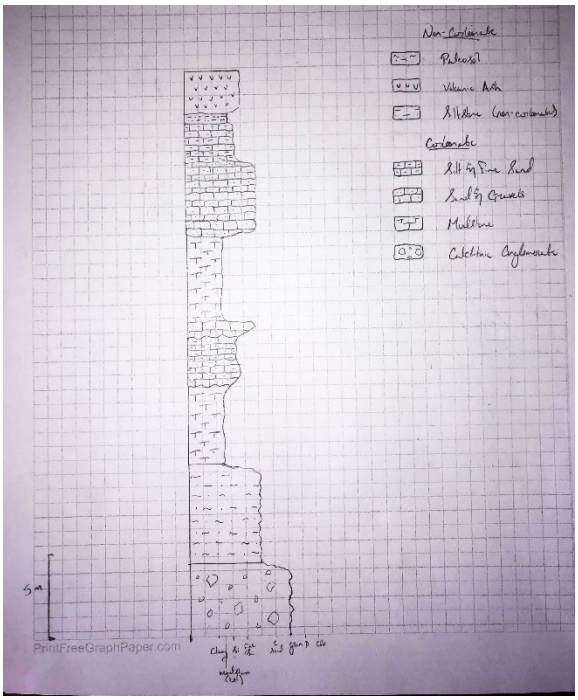

Figure 2: Stratigraphic Column of the Camp Davis Formation.

Materials and Methods

Three outcrop samples were taken from the exposed ridge of the Camp Davis Formation directly to north of the University of Michigan Camp Davis Field Station (Fig. 3). Sample CD-1 represents the lowest stratigraphic part of the Formation, taken approximately 5 meters above the contact with the lower conglomeratic subunit. Sample CD-3 represents the lithology approximately within the central part of the Formation, whereas CD-2 is the highest stratigraphic level of the carbonate subunit of the Camp Davis Fm. A fourth sample (65-001) was provided by Dr. Carl Drummond from his collection, but was not used in his earlier study (Drummond et al., 1993). Its stratigraphic position is unknown, yet it was collected at this site.

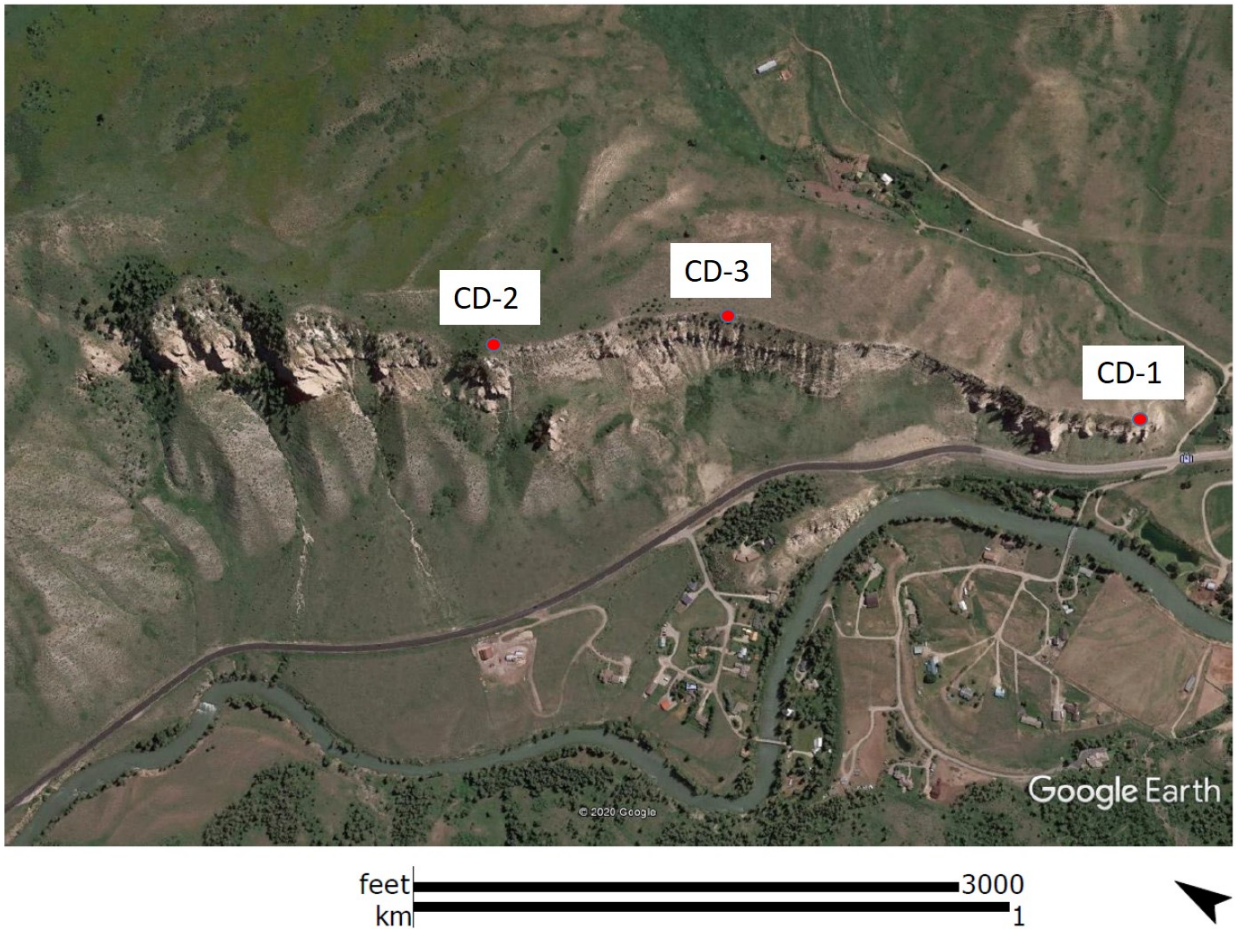

Figure 1: Satellite image of the outcrop of the Camp Davis Fm. occurring north of US 191. For reference, CD-2 GPS location is 43o18'42.99"N 10o40'32.05"W.

The four samples were analyzed with conventional stable isotope techniques for their $\delta^{18}O$ and $\delta^{13}C$ content. Samples CD-1 and CD-3 are tan to brown homogenous micrite with voids filled by clear calcite spar (Fig. 4A and 4C). Sample CD-2 is distinct from these, with brown micrite surrounding intraclasts (Fig. 4B). These clasts are likely pre-existing Paleozoic limestone displaced due to uplift of the Hoback Fault. Sample 65-001 is distinct from the previous three samples (Figure 4D). It contains clear spar, a dark brown cement, and light brown micrite, along

with oncoliths formed around nuclei of micritic limestone. A description of each sample is provided below along with photographs of the slabbed surface that was microsampled for analysis.

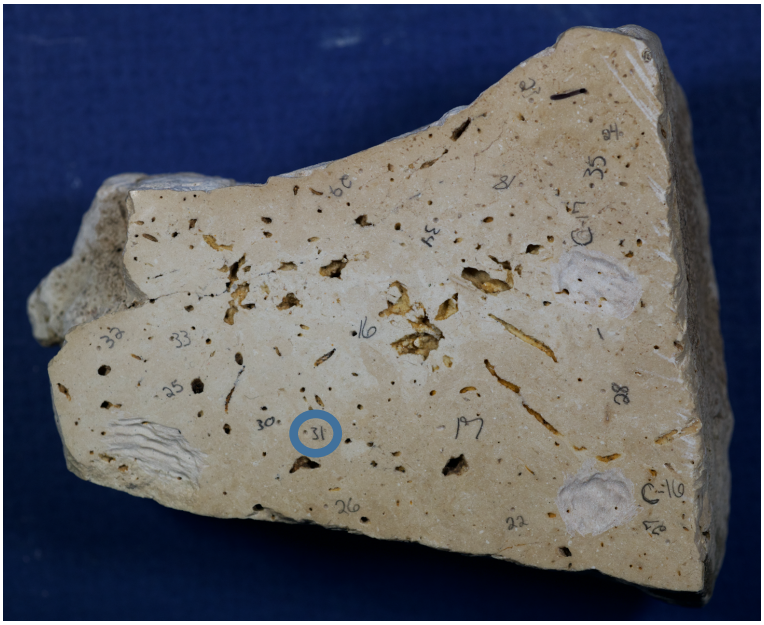

Figure 2A: Sample CD-1. This sample is characterized as a largely homogeneous micritic limestone containing sparse disseminated intraclasts. Note the open rootlets that are distributed throughout the sample. Numbers reflect areas that were sampled for discrete $\delta^{18}O$ and $\delta^{13}C$ analyses. Sample areas were generally shallow drill pits less than 0.5mm in diameter. For example, the spot adjacent to sample #31 is typical in size (circled area). Sample length is 13mm.

Figure 4B: Sample CD-2. This sample is micritic limestone containing both intraclasts (clasts derived from intraformational sources potentially in response to desiccation) and intraclasts from allogenic sources (likely Mesozoic and Paleozoic limestone undergoing erosion from the uplifted block of the Hoback Fault. Sample length is 16 mm

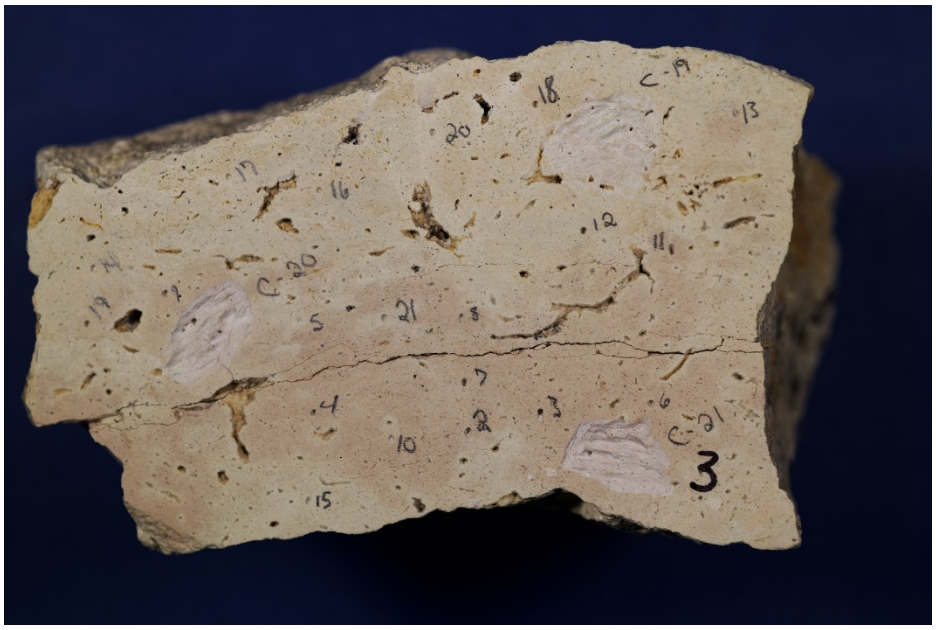

Figure 4C: Sample CD-3. This sample is very similar to Sample 1 in that it comprise a relatively homogenous micritic limestone that has been mottled by rootlets represented by elongate voids. Notably, it is devoid of intraclasts and lithoclasts. Scale length is 12 mm.

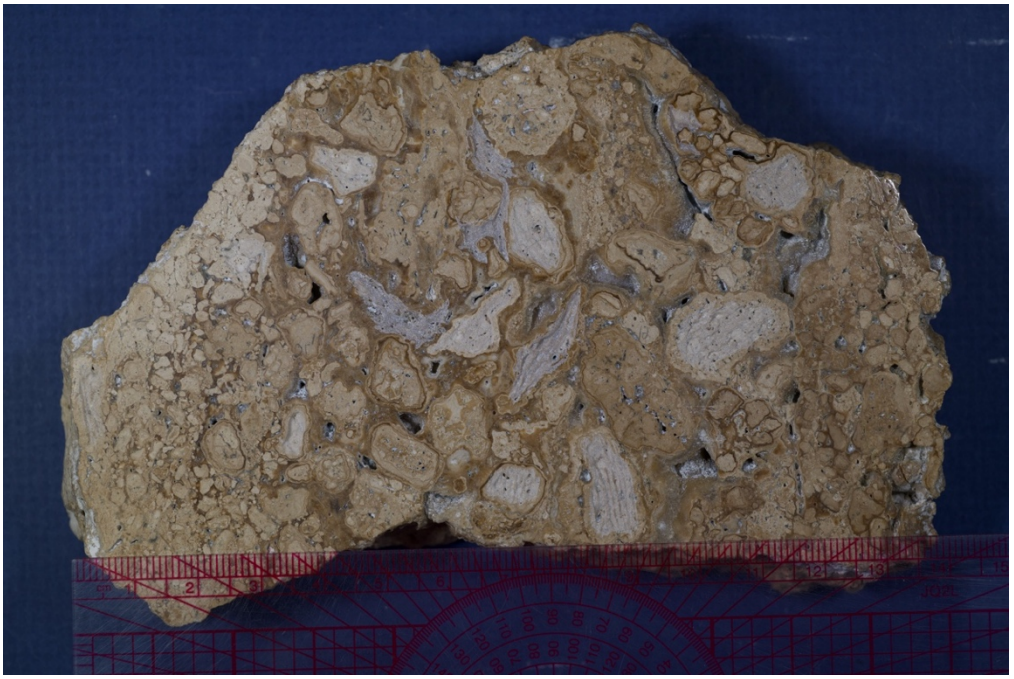

Figure 4D: Sample 65-1000 was collected from the same locality as Samples 1-3, though lower within the stratigraphic section. It is characterized as an oncolitic grainstone. These "oncoliths" are algally-coated clasts where the nuclei represent intraclasts of micritic limestone. The darker outer coatings represent synsedimentary isopachous calcite cements lining pores between clasts. A final stage of fine clear prismatic calcite cements partially fill remaining porosity. Sample provided by Carl Drummond. Sample length is 20 mm.

An essential part of this research is determining the variation in $\delta^{18}O$ and $\delta^{13}C$ present within each sample. Specifically, individual rock components, lithoclasts, cements, and matrix micrite were microsampled utilizing a 0.5mm dental burr attached to a dental laboratory handpiece. Samples were taken from polished slabs and transferred to metal capsules for storage prior to analysis. Samples sizes were typically 50 to 100 micrograms in size. Analysis of these sample

powders was performed using a Kiel IV automated extractions system coupled to the inlet of a Delta V Isotope Ratio Mass Spectrometer. A linear correction transfer function was used to convert laboratory measured values to VPDB based on a linear regression analysis of powdered NBS-19 and NBS-18 standards. This correction simultaneously accommodates for reference gas composition and acid fractionation effects. Analytical precision based on replication of these standards is better than 0.1‰ for both $\delta^{13}C$ and $\delta^{18}O$.

Clumped isotope analysis of the four samples was intended using the method of Defliese et al. (2015). Powder samples were taken from the larger rock using a drill and were approximately 15 mg each to allow for 3 duplicates of 5 mg to be run. Powder samples were then run through the custom extraction system pictured in Figure 5.

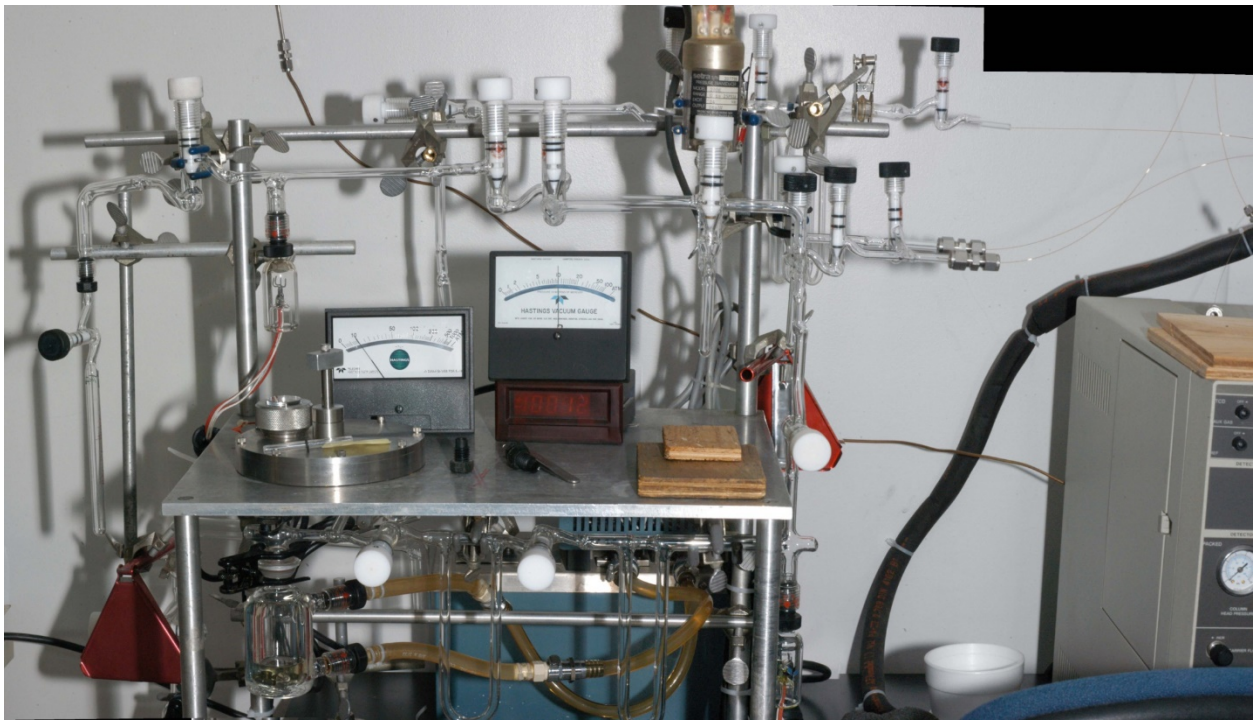

Figure 5: Extraction System for Clumped Isotope Analysis.

In this system, carbonate powder is reacted with 103% phosphoric acid at 70ºC to produce CO_2 and H_2O. The resulting gases are then cryogenically separated to remove water and other contaminants. Water is removed from the gas at -90°C, and remaining organic impurities are separated out by transferring the gas through a column of PoraPak Q resin at -18°C (Defliese and Lohmann, 2015). These gas samples are archived and will be eventually analyzed Purified sample gases will be analyzed on a Thermo Electron MAT 253 configured to measure masses 44, 45, 46, 47, 48 and 49. Δ47 values will be calculated from measured δ47 values utilizing the approach of Petersen et. al (2019). All Δ47 values will be corrected to the Universal Reference Frame based on analysis of heated gases and CO_2 equilibrated with water at 25ºC according to the procedures of Dennis et al. (2011)

Results

Conventional Carbon and Oxygen Analyses

There is a significant difference between the isotope values reported by Drummond et al. when completing their paleoelevation study and those completed as part of this study (Figure 6). The $\delta^{18}O$ values measured by Drummond et al. (1993) sit at an average of -27.6‰. The measured $\delta^{18}O$ values for this study are detailed in the appendix and average to -16.7‰. The values for each specific component also differ greatly. For example, the three very negative $\delta^{13}C$ values in Drummond et al. (1993) results were taken from clear spar, while Figure 8 shows clear spar from 65-001 to be very positive in $\delta^{13}C$. Additionally, micrite in their study has an average $\delta^{18}O$ of -26.9‰, almost 10‰ more negative than this study's micrite average of -17.3‰.

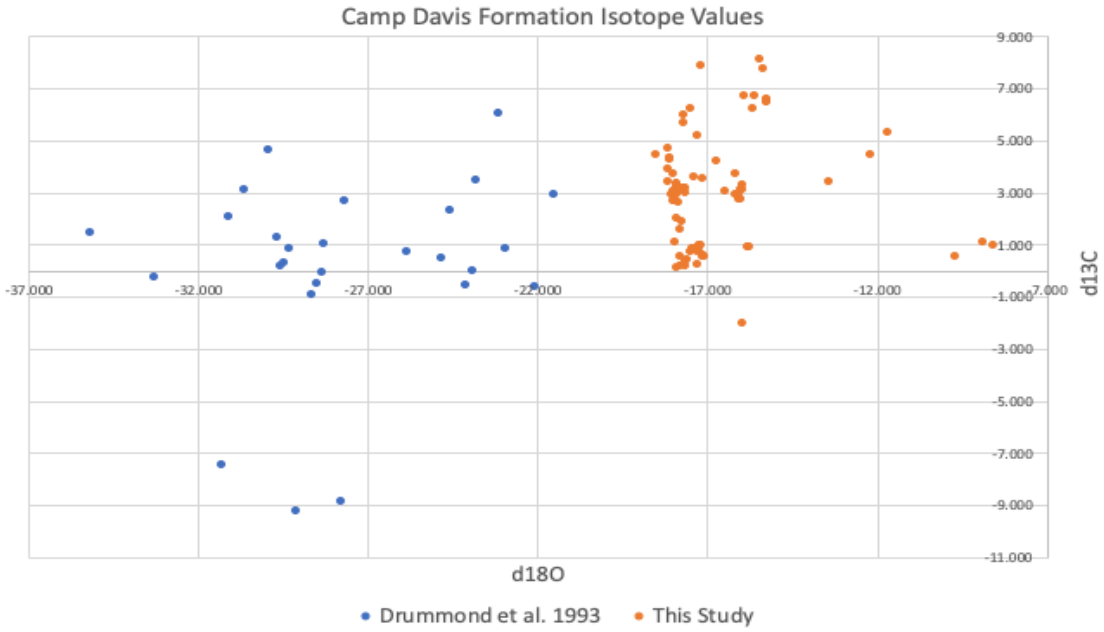

Figure 6: Comparison with of this study with Drummond et al. 1993. No data points from overlap with one another, which is unexpected given that the same study area was used. Additionally, Drummond et al. measured values that were much more negative than anything found in this study.

Figure 7 illustrates this study's isotope values based on individual samples. Two groups can be defined from the measured oxygen isotope values: a group with $\delta^{18}O$ of approximately -18.0‰, and a group with $\delta^{18}O$ of approximately -16.0‰. While three different samples constitute the more negative group, the second group is comprised solely by sample CD-2. The more depleted samples, CD-1, CD-3, and 65-001, all sit with similar $\delta^{18}O$ values. None of these samples exhibit as much compositional variation as CD-2, being generally tightly clustered in terms of oxygen. $\delta^{13}C$ values for all four samples vary greatly, however; they range from -2.0 to -8.0‰ for CD-2, and from 0.0 to -8.0‰ for CD-1, CD-3, and 65-001.

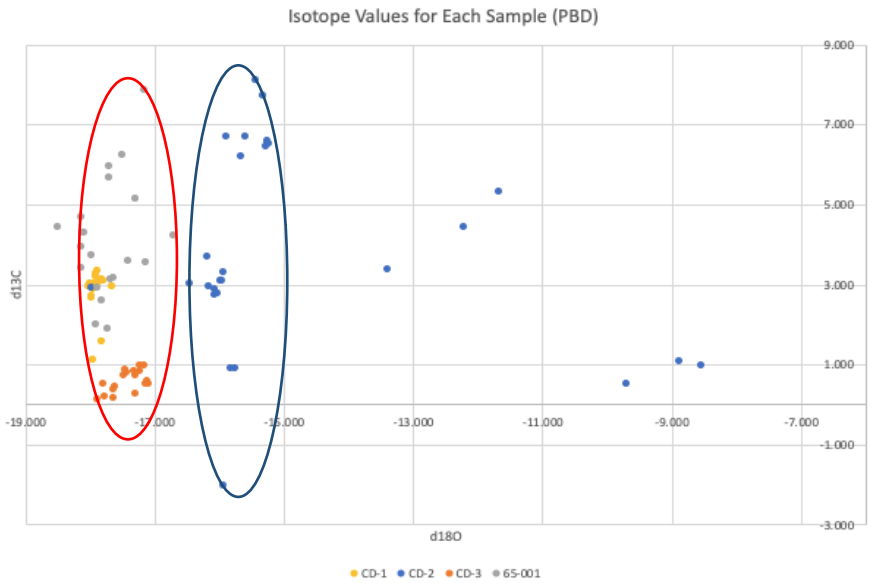

Figure 7: Isotope values separated into the four samples used in this study. Group one, composed of the depleted samples CD-1, CD-3, and 65-001, is circled in red. Group 2, composed of enriched sample CD-2, is circled in dark blue. Outliers belong to CD-2 and are shown in further detail in Figure 9.

With the exception of a singular clast in CD-1, the three more depleted samples were composed only of matrix micrite, spar, and cement (Figure 8). They sit at an average $\delta^{18}O$ value of 17.7‰, with sample 65-001 exhibiting the largest oxygen and carbon variation in the group. CD-1 and CD-3 are more tightly clustered with relatively little variation. Micrite from CD-3 has the most negative carbon values, while cements and spar have the most positive carbon values.

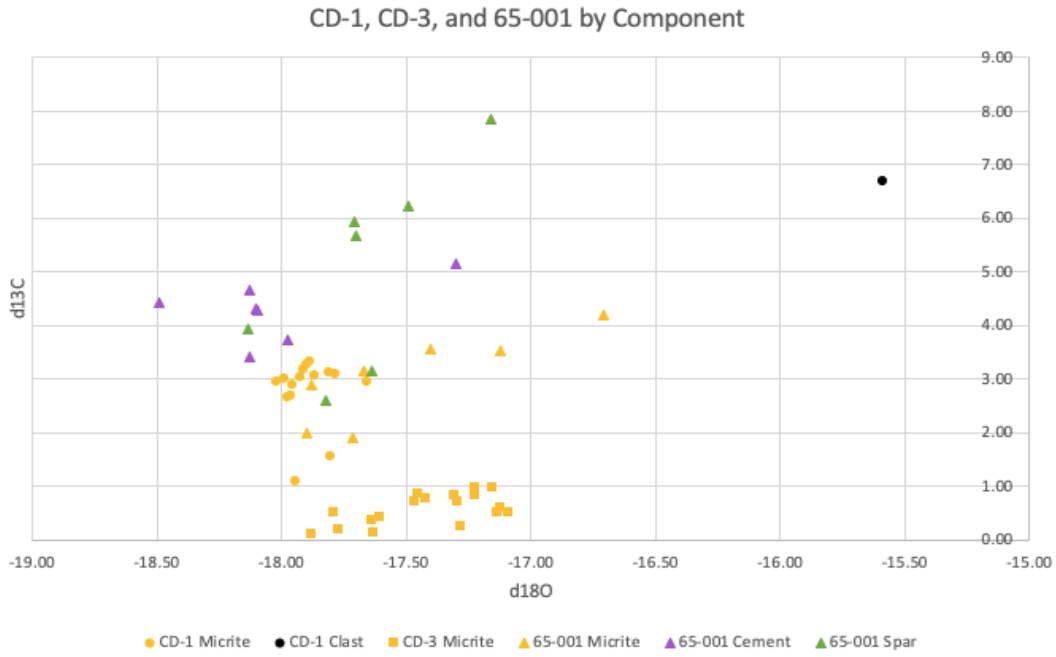

Figure 8: Comparison of $\delta^{18}O$-depleted samples by component. Generally, there is much more variation in $\delta^{13}C$ than in $\delta^{18}O$, with all samples having approximately the same $\delta^{18}O$ variation in their micrite.

CD-2, on the other hand, is clearly distinct from the group discussed above (Figure 9). It is the only sample to have an abundance of lithoclasts, and its micrite matrix is darker in color than the CD-1 and CD-3. Its $\delta^{18}O$ values for micrite sit at an average of -16.2‰, more enriched than any of the previous three samples. Additionally, many of CD-2's clasts possess $\delta^{18}O$ values greater than -14‰. Despite the variation in $\delta^{18}O$, these data show micrite defining a narrow range in $\delta^{13}C$, similar to the other three samples. In fact, the micrite in CD-2 has $\delta^{13}C$ values almost exactly matching those of CD-1. However, clasts in CD-2 represent both positive and negative $\delta^{13}C$ values, with a range spanning the whole spread of carbon values for CD-1, CD-3, and 65-001.

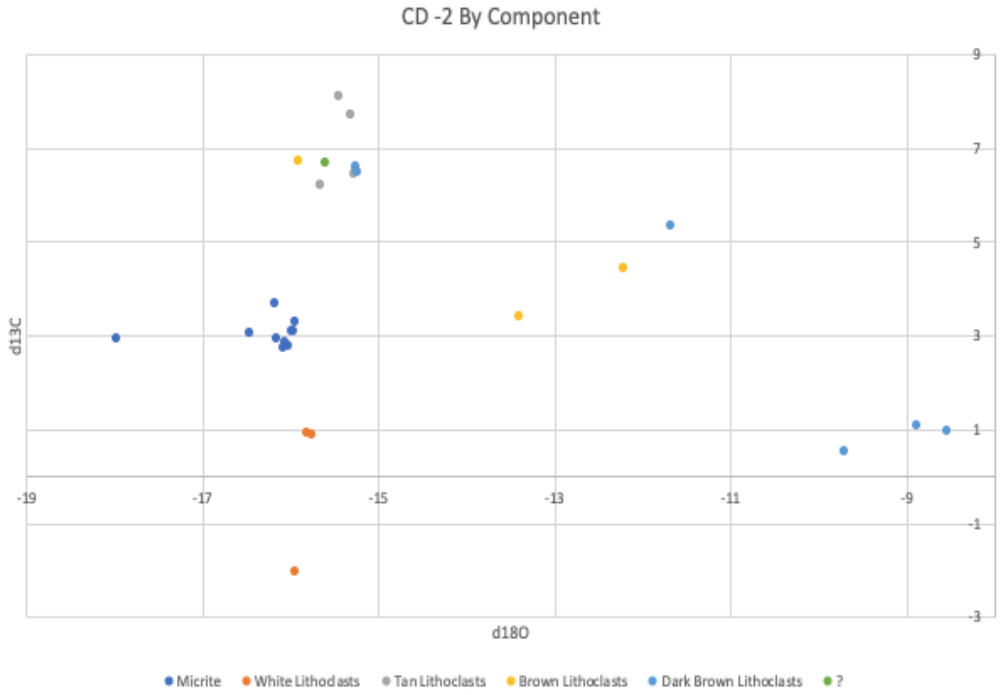

Figure 9: Analysis of sample CD-2 by component. The micrite in this sample is clustered in the same way as that in the depleted samples are, with clast data points spread out around it. The green data point may have been a split measurement of a clast.

Interpretation and Discussion

A number of conclusions can be drawn about the Camp Davis Fm. from the $\delta^{18}O$ values measured in this study. The two compositional groups based on $\delta^{18}O$ indicate that environmental conditions changed significantly between formation of the more depleted samples and sample CD-2, which lies near the top of the limestone member. The discrepancy may be explained by colder temperatures during the formation of limestones represented by CD-2. At colder temperatures, precipitation includes more ^{18}O to be incorporated into the carbonate. For the magnitude of difference seen between the groups seen in this study (~2‰), the temperature would have had to be at least 10°C colder than during the depleted samples' formation (Hren and Sheldon, 2012).

Carbonate generally only precipitates during the warm summer months (Hren and Sheldon, 2012), and thus precipitation at 10°C or 15°C seems unlikely.

A period of lake restriction and evaporation during formation of CD-2 could also explain the separation between the populations. A more evaporative environment could cause such enriched values as the vapor phase preferentially removes ^{16}O out from lake water. Very early lithification indicated for CD-2 is further evidence of such a setting, as periods of desiccation and reworking are necessary in the development of lithoclasts. These clasts cover a range of oxygen content, with some approaching $\delta^{18}O$ values of -10‰. However, CD-2 also contains lithoclasts with $\delta^{18}O$ values similar to that of the enclosing micrite in the sample, just over -15‰. All evidence suggests that these lithoclasts are intraformational, derived from the Camp Davis Fm. itself, through periodic desiccation and lithification of lake micrites. Reworking of lithoclasts could occur by erosion by surface waves during periods of resubmergence. This also seems plausible given that sample CD-2 represents the stratigraphically highest occurrence of limestone prior to the shift to upper Camp Davis Fm. lithologies comprising volcanic ash deposited in a more arid terrestrial environment.

Table 1: Calculated $\delta^{18}O_w$ values at a given temperature and $\delta^{18}O_{Cc}$ value. $\delta^{18}O$ was calculated using Equations 2 and 3.

	$d^{18}O_{cc}$ (‰)	$d^{18}O_w$ @T (‰)	$d^{18}O_w$ @T (‰)	$d^{18}O_w$ @T (‰)
Temperature		20	25	30
CD-1 Minimum	-18.02	-17.05	-16.00	-14.99
Maximum	-17.66	-16.69	-15.64	-14.63
CD-2 Minimum	-17.96	-16.99	-15.94	-14.93
Maximum	-15.94	-14.97	-13.91	-12.90
CD-3 Minimum	-17.88	-16.91	-15.86	-14.85
Maximum	-17.09	-16.12	-15.06	-14.06
65-001 Minimum	-17.90	-16.93	-15.88	-14.87
Maximum	-16.71	-15.74	-14.68	-13.68
All Average	-17.34	-16.36	-15.31	-14.30
Enriched Group Average	-16.23	-15.26	-14.20	-13.19
Depleted Group Average	-17.61	-16.64	-15.59	-14.58
Total Average	-17.33	-16.36	-15.30	-14.29
Std. Deviation	0.665	0.666	0.667	0.667

Though all four samples have a low degree of variability in oxygen overall, their carbon variability is high, ranging from approximately -2.04‰ to 9.09‰. Variation in $\delta^{13}C$ values is much larger than the 4‰ difference between our highest and lowest $\delta^{18}O$ values. Such high carbon variability is likely due to the relative ease of changing carbon isotope content in water relative to $\delta^{18}O$. $\delta^{13}C$ values are generally an artifact of biotic productivity – high productivity can result in shift toward more positive $\delta^{13}C$ values, and vice versa. Depending on the productivity at the time of carbonate formation, a broad range of $\delta^{13}C$ values would be expected in a lacustrine system.

This is in contrast to the extremely positive $\delta^{13}C$ values observed in 65-001, which contains abundant synsedimentary cements. Their high $\delta^{13}C$ values are associated with dark brown colored fibrous cements filling primary porosity. Such enriched $\delta^{13}C$ values suggest cement formation under conditions of organic fermentation, or the breakdown of organic material in an anoxic environment. Organic fermentation produces methane which sequesters ^{12}C from the system while also producing ^{13}C enriched HCO_3^- that leads to the formation of cements. In this case, the process would leave a high amount ^{13}C available to be incorporated into carbonate. However, CD-2 also includes clasts with $\delta^{13}C$ values close to those measured for the cements. The reason for the clasts' values is unknown, but likely not related to fermentation, illustrating that multiple biotic and abiotic processes can end up with the same $\delta^{13}C$ values.

Using the $\delta^{18}O$ values measured from the four samples, we were able to calculate what the isotopic composition of the water ($\delta^{18}O_w$) would have been at the time of carbonate formation. $\delta^{18}O_w$ was calculated over a range of temperatures from 20°C to 30°C with Equations 2 and 3 (above). These temperatures were chosen because carbonate generally forms during the spring and summer months, when the weather is relatively warm (Hren and Shedon, 2012). Table 1 shows the values used for these calculations, as well as the resulting $\delta^{18}O_w$ values at a specific temperature.

The most negative $\delta^{18}O_w$ value, -17.05‰, comes from the calculation using the minimum $\delta^{18}O$ value of micrite in sample CD-1 at 20 °C. The most positive value, -12.9‰, predictably comes from the maximum $\delta^{18}O$ value of CD-2 micrite at 30°C. The averages of depleted and enriched carbonate micrite populations are separated by more than 1‰, though calculated water compositions for both provide estimates similar to the isotopic composition of modern meteoric water (-16.5‰) of the Jackson Hole Wyoming region (Drummond et al., 1993). Assuming that these types of micrite are compositionally dominant in the formation, the small difference implies little to no elevation change for the Camp Davis Fm. over the course of its deposition or relative to present day. An additional comparison with $\delta^{18}O_w$ values calculated by Dutton et al. (2005) draws a similar result. The Green River runs close to the Camp Davis Fm.'s location and sits at a comparable elevation. Its current $\delta^{18}O_w$ to be -15.6‰, matching the average for depleted micrite in this study. The two values serve as more evidence that the paleoelevation of the Camp Davis Fm. is likely not too different from its current state.

None of the $\delta^{18}O_w$ estimates provided by this study are more negative than -17.1‰, which was unexpected when this study began given the previous paleoelevation study by Drummond et al. (1993). While the Drummond et al. (1993) study yielded average $\delta^{18}O_w$ of -26.74‰ and -24.64‰ (20 °C and 30 °C, respectively), measured values of this study average of -16.36‰ and -14.29‰ for those same temperatures. The approximately 10‰ difference means that both studies will come to contradicting conclusions when quantifying paleoelevation. All evidence collected here places the Camp Davis Fm. at an elevation of approximately 2.5 km in the late Miocene (Figure 10), very close to the mean present-day elevation of the Gros Ventre mountains (2.8 km; Drummond et al., 1993). However, Drummond et al. (1993) determined that the formation was "0.5 to 1.2 km higher than at present", necessitating some major erosion or tectonic event, or perhaps a combination of both.

A possible explanation for this discrepancy could be that the majority of samples examined by Drummond et al. (1993) were taken from an unrepresentative portion of the formation. Their reported values do not overlap at all with this study (Figure 6), and in fact our $\delta^{18}O_w$ values sit at the lowest end of their reported numbers for non-evaporitic lakes. As this study gathered samples from only the upper part of the Camp Davis Fm., collecting samples from a wider portion of formation is a viable step to see if any $\delta^{18}O_w$ values match those found by Drummond et al. (1993). Future analysis should also provide data generated through the use of clumped isotope analysis, which would provide an independent measure of temperature at formation. With a unique determination of temperature, unique calculations of water compositions can be performed and paleoaltimetry estimates can be more accurately constrained.

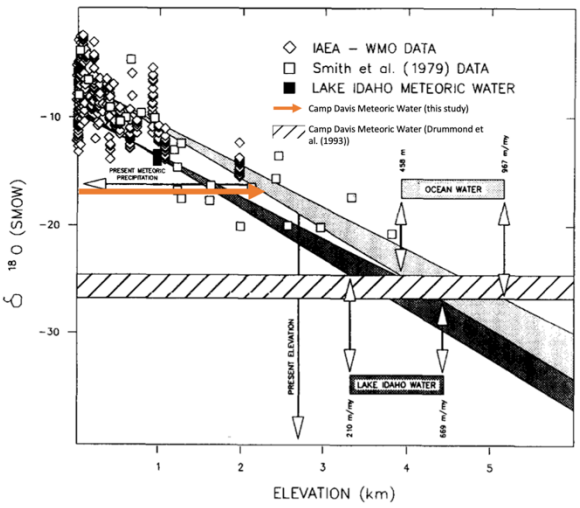

Figure 10: Details the relationship of $\delta^{18}O$ to elevation. The black line represents $\delta^{18}O$-elevation dependence should all water be derived from western regional lakes, and the light grey line depicts the relationship should all water be derived from oceanic sources. The orange arrow shows this study's mean elevation based on the average $\delta^{18}O$ values of 16.6‰. Figure is modified from Drummond et al. 1993.

References Cited

Davis, Rhonda L., and Bruce H. Wilkinson. *Sedimentology and Petrology of Freshwater Lacustrine Carbonate: Mid-Tertiary Camp Davis Formation, Northwestern Wyoming*. 1983, p. 11.

Defliese, William F., and Kyger C. Lohmann. "Non-Linear Mixing Effects on Mass-47 CO2 Clumped Isotope Thermometry: Patterns and Implications." *Rapid Communications in Mass* Spectrometry, vol. 29, no. 9, 2015, pp. 901–09. Wiley Online Library, doi:10.1002/rcm.7175.

Dennis, K. J.,Affek, H. P.,Passey, B. H.,Schrag, D. P., &Eiler, J. M."Defining an absolute reference frame for 'clumped' isotope studies of CO_2." 2011, Geochimica et Cosmochimica Acta, 75(22), 7117–7131

Drummond, Carl N., et al. "Effect of Regional Topography and Hydrology on the Lacustrine Isotopic Record of Miocene Paleoclimate in the Rocky Mountains." *Palaeogeography, Palaeoclimatology, Palaeoecology*, vol. 101, no. 1–2, Mar. 1993, pp. 67–79. *DOI.org (Crossref)*, doi:10.1016/0031-0182(93)90152-9.

Dutton, Andrea, et al. "Spatial Distribution and Seasonal Variation in ^{18} O/ ^{16} O of Modern Precipitation and River Water across the Conterminous USA." *Hydrological Processes*, vol. 19, no. 20, Dec. 2005, pp. 4121–46. *DOI.org (Crossref)*, doi:10.1002/hyp.5876.

Eiler, John M. "'Clumped-Isotope' Geochemistry—The Study of Naturally-Occurring, Multiply-Substituted Isotopologues." *Earth and Planetary Science Letters*, vol. 262, no. 3–4, Oct. 2007, pp. 309–27. *DOI.org (Crossref)*, doi:10.1016/j.epsl.2007.08.020.

Garzione, C., et al. "Carbonate Oxygen Isotope Paleoaltimetry: Evaluating the Effect of Diagenesis on Paleoelevation Estimates for the Tibetan Plateau." *Palaeogeography, Palaeoclimatology, Palaeoecology*, vol. 212, no. 1–2, Sept. 2004, pp. 119–40. *DOI.org (Crossref)*, doi:10.1016/S0031-0182(04)00307-4.

Gébelin, Aude, et al. "The Miocene Elevation of Mount Everest." *Geology*, vol. 41, no. 7, July 2013, pp. 799–802. *DOI.org (Crossref)*, doi:10.1130/G34331.1.

Hough, Brian G., et al. "Calibration of the Clumped Isotope Geothermometer in Soil Carbonate in Wyoming and Nebraska, USA: Implications for Paleoelevation and Paleoclimate Reconstruction." *Earth and Planetary Science Letters*, vol. 391, Apr. 2014, pp. 110–20. *DOI.org (Crossref)*, doi:10.1016/j.epsl.2014.01.008.

Hren, Michael T., and Nathan D. Sheldon. "Temporal Variations in Lake Water Temperature: Paleoenvironmental Implications of Lake Carbonate Δ18O and Temperature Records." *Earth and Planetary Science Letters*, vol. 337–338, July 2012, pp. 77–84. *DOI.org (Crossref)*, doi:10.1016/j.epsl.2012.05.019.

Jasechko, S., et al. "Late-Glacial to Late-Holocene Shifts in Global Precipitation δ ^{18} O." *Climate of the Past*, vol. 11, no. 10, Oct. 2015, pp. 1375–93. *DOI.org (Crossref)*, doi:10.5194/cp-11-1375-2015.

Lechler, Alex R., et al. "Paleoelevation Estimates for the Northern and Central Proto–Basin and Range from Carbonate Clumped Isotope Thermometry." *Tectonics*, vol. 32, no. 3, 2013, pp. 295–316. *Wiley Online Library*, doi:10.1002/tect.20016.

Mulch, A., and C. P. Chamberlain. "Stable Isotope Paleoaltimetry in Orogenic Belts The Silicate Record in Surface and Crustal Geological Archives." *Reviews in Mineralogy and Geochemistry*, vol. 66, no. 1, Oct. 2007, pp. 89–118. *DOI.org (Crossref)*, doi:10.2138/rmg.2007.66.4.

Mulch, Andreas. "Stable Isotope Paleoaltimetry and the Evolution of Landscapes and Life." *Earth and Planetary Science Letters*, vol. 433, Jan. 2016, pp. 180–91. *DOI.org (Crossref)*, doi:10.1016/j.epsl.2015.10.034.

Passey, Benjamin H., et al. "Triple Oxygen Isotopes in Biogenic and Sedimentary Carbonates." *Geochimica et Cosmochimica Acta*, vol. 141, Sept. 2014, pp. 1–25. *DOI.org (Crossref)*, doi:10.1016/j.gca.2014.06.006.

Quade, J., et al. "Paleoelevation Reconstruction Using Pedogenic Carbonates." *Reviews in Mineralogy and Geochemistry*, vol. 66, no. 1, Oct. 2007, pp. 53–87. *DOI.org (Crossref)*, doi:10.2138/rmg.2007.66.3.

Rowley, David B., et al. "A New Approach to Stable Isotope-Based Paleoaltimetry: Implications for Paleoaltimetry and Paleohypsometry of the High Himalaya since the Late Miocene." *Earth and Planetary Science Letters*, vol. 188, no. 1–2, May 2001, pp. 253–68. *DOI.org (Crossref)*, doi:10.1016/S0012-821X(01)00324-7.

Rowley, David B., and Carmala N. Garzione. "Stable Isotope-Based Paleoaltimetry." *Annual Review of Earth and Planetary Sciences*, vol. 35, no. 1, 2007, pp. 463–508. *Annual Reviews*, doi:10.1146/annurev.earth.35.031306.140155.

Wing, Scott L., and Guy J. Harrington. “Floral Response to Rapid Warming in the Earliest Eocene and Implications for Concurrent Faunal Change.” *Paleobiology*, vol. 27, no. 3, Paleontological Society, 2001, pp. 539–63. JSTOR.

Appendix: $\delta^{13}C$ and $\delta^{18}O$ values for each sample used in this study. Component is also shown for comparison.

ID#	Sample	Component	$\delta^{13}C$	$\delta^{18}O$
CD - 1 - 1	CD-1	Tan Micrite	2.95	-17.66
CD - 1 - 16	CD-1	Clast	6.68	-15.59
CD - 1 - 17	CD-1	White Micrite	2.94	-18.02
CD - 1 - 22	CD-1	Brown/Tan Micrite	3.01	-17.99
CD - 1 - 24	CD-1	Brown/Tan Micrite	1.10	-17.94
CD - 1 - 25	CD-1	Tan Micrite	3.07	-17.87
CD - 1 - 26	CD-1	Brown Micrite	2.89	-17.96
CD - 1 - 27	CD-1	Brown Micrite	2.68	-17.96
CD - 1 - 28	CD-1	Brown Micrite	2.67	-17.97
CD - 1 - 29	CD-1	Brown Micrite	3.19	-17.91
CD - 1 - 30	CD-1	Tan Micrite	3.03	-17.92
CD - 1 - 31	CD-1	Brown Micrite	3.13	-17.81
CD - 1 - 32	CD-1	Tan Micrite	3.27	-17.90
CD - 1 - 33	CD-1	Tan Micrite	3.08	-17.78
CD - 1 - 34	CD-1	Brown Micrite	3.33	-17.89
CD - 1 - 35	CD-1	Brown Micrite	1.56	-17.81
CD - 2 - 2	CD-2	White Lithic Glass	0.91	-15.81
CD - 2 - 2	CD-2	White Lithic Glass	0.89	-15.74
CD - 2 - 3	CD-2	Brown Lithic Glass	4.43	-12.21
CD - 2 - 3	CD-2	Brown Lithic Glass	3.38	-13.40
CD - 2 - 4	CD-2	Tan Lithic Glass	6.52	-15.25
CD - 2 - 4	CD-2	Tan Lithic Glass	6.44	-15.26
CD - 2 - 5	CD-2	Tan Lithic Glass	6.21	-15.65
CD - 2 - 6	CD-2	Clast	7.71	-15.32
CD - 2 - 7	CD-2	Clast	8.09	-15.44
CD - 2 - 8	CD-2	Clast	6.50	-15.23
CD - 2 - 9	CD-2	Clast	6.58	-15.25
CD - 2 - 10	CD-2	Tan Micrite	2.93	-16.15
CD - 2 - 11	CD-2	Tan Micrite	3.03	-16.46
CD - 2 - 12	CD-2	Clast	0.95	-8.54
CD - 2 - 12	CD-2	Clast	1.07	-8.87
CD - 2 - 13	CD-2	Brown Micrite	2.74	-16.07
CD - 2 - 13	CD-2	Brown Micrite	2.76	-16.02
CD - 2 - 14	CD-2	White Lithic Glass	-2.04	-15.93
CD - 2 - 15	CD-2	Clast	6.68	-15.59
CD - 2 - 18	CD-2	Dark Brown Micrite	2.91	-17.96
CD - 2 - 19	CD-2	Clast	0.51	-9.69

CD - 2 - 20	CD-2	Brown Lithic Glass	6.70	-15.90
CD - 2 - 21	CD-2	Tan Micrite	3.68	-16.17
CD - 2 - 36	CD-2	Clast	5.32	-11.67
CD - 2 - 37	CD-2	Light Brown Micrite	3.08	-15.96
CD - 2 - 38	CD-2	Light Brown Micrite	3.30	-15.94
CD - 2 - 39	CD-2	Light Brown Micrite	3.10	-15.99
CD - 2 - 40	CD-2	Dark Brown Micrite	2.87	-16.06
CD - 3 - 2	CD-3	Pink Micrite	0.98	-17.22
CD - 3 - 3	CD-3	Pink Micrite	0.51	-17.14
CD - 3 - 4	CD-3	Pink Micrite	0.59	-17.12
CD - 3 - 6	CD-3	Pink Micrite	0.53	-17.09
CD - 3 - 7	CD-3	Pink Micrite	0.98	-17.16
CD - 3 - 8	CD-3	Pink Micrite	0.83	-17.22
CD - 3 - 9	CD-3	Pink Micrite	0.43	-17.60
CD - 3 - 11	CD-3	Pink Micrite	0.82	-17.31
CD - 3 - 12	CD-3	Tan Micrite	0.25	-17.28
CD - 3 - 13	CD-3	Tan Micrite	0.86	-17.45
CD - 3 - 14	CD-3	Tan Micrite	0.79	-17.42
CD - 3 - 15	CD-3	Tan Micrite	0.72	-17.46
CD - 3 - 16	CD-3	Light Brown Micrite	0.11	-17.88
CD - 3 - 17	CD-3	Light Brown Micrite	0.15	-17.63
CD - 3 - 18	CD-3	Light Brown Micrite	0.36	-17.64
CD - 3 - 19	CD-3	Light Brown Micrite	0.52	-17.79
CD - 3 - 20	CD-3	Tan Micrite	0.18	-17.77
CD - 3 - 21	CD-3	Tan Micrite	0.72	-17.30
65-001 - 1	65-001	Dark Brown Cement	5.15	-17.30
65-001 - 2	65-001	Dark Brown Cement	3.74	-17.98
65-001 - 3	65-001	Dark Brown Cement	4.67	-18.13
65-001 - 4	65-001	Dark Brown Cement	4.29	-18.10
65-001 - 5	65-001	Dark Brown Cement	4.42	-18.49
65-001 - 6	65-001	Dark Brown Cement	4.30	-18.10
65-001 - 7	65-001	Dark Brown Cement	3.41	-18.13
65-001 - 8	65-001	Light Brown Micrite	3.54	-17.12
65-001 - 9	65-001	Light Brown Micrite	1.89	-17.72
65-001 - 10	65-001	Light Brown Micrite	2.01	-17.90
65-001 - 11	65-001	Light Brown Micrite	2.90	-17.88
65-001 - 12	65-001	Light Brown Micrite	3.14	-17.67
65-001 - 13	65-001	Light Brown Micrite	4.21	-16.71
65-001 - 14	65-001	Light Brown Micrite	3.57	-17.40
65-001 - 15	65-001	Clear Spar	5.95	-17.71

65-001 - 16	65-001	Clear Spar	2.60	-17.82
65-001 - 17	65-001	Clear Spar	7.85	-17.16
65-001 - 18	65-001	Clear Spar	6.22	-17.49
65-001 - 19	65-001	Clear Spar	3.15	-17.64
65-001 - 20	65-001	Clear Spar	5.67	-17.70
65-001 - 21	65-001	Clear Spar	3.92	-18.13